1521-0103/364/3/494–503$35.00
THE JOURNAL OF PHARMACOLOGY AND EXPERIMENTAL THERAPEUTICS

https://doi.org/10.1124/jpet.117.244129
J Pharmacol Exp Ther 364:494–503, March 2018

Triple Angiokinase Inhibitor Nintedanib Directly Inhibits Tumor Cell Growth and Induces Tumor Shrinkage via Blocking Oncogenic Receptor Tyrosine Kinases[S]

Frank Hilberg, Ulrike Tontsch-Grunt, Anke Baum, Anh T. Le, Robert C. Doebele, Simone Lieb, Davide Gianni, Tilman Voss, Pilar Garin-Chesa, Christian Haslinger, and Norbert Kraut

Boehringer Ingelheim RCV GmbH Co KG, Vienna, Austria (F.H., U.T.-G., A.B., S.L., D.G., T.V., P.G.-C., C.H., N.K.); University of Colorado, School of Medicine, Division of Medical Oncology, Aurora, Colorado (A.T.L., R.C.D.); and AstraZeneca - Innovative Medicines and Early Development, Discovery Sciences, Cambridge Science Park, Milton, Cambridge (D.G.)

Received July 25, 2017; accepted December 11, 2017

ABSTRACT

The triple-angiokinase inhibitor nintedanib is an orally available, potent, and selective inhibitor of tumor angiogenesis by blocking the tyrosine kinase activities of vascular endothelial growth factor receptor (VEGFR) 1–3, platelet-derived growth factor receptor (PDGFR)-α and -β, and fibroblast growth factor receptor (FGFR) 1–3. Nintedanib has received regulatory approval as second-line treatment of adenocarcinoma non–small cell lung cancer (NSCLC), in combination with docetaxel. In addition, nintedanib has been approved for the treatment of idiopathic lung fibrosis. Here we report the results from a broad kinase screen that identified additional kinases as targets for nintedanib in the low nanomolar range. Several of these kinases are known to be mutated or overexpressed and are involved in tumor development (discoidin domain receptor family, member 1 and 2, tropomyosin receptor kinase A (TRKA) and C, rearranged during transfection proto-oncogene [RET proto oncogene]), as well as in fibrotic diseases (e.g., DDRs). In tumor cell lines displaying molecular alterations in potential nintedanib targets, the inhibitor demonstrates direct antiproliferative effects: in the NSCLC cell line NCI-H1703 carrying a PDGFRα amplification (ampl.); the gastric cancer cell line KatoIII and the breast cancer cell line MFM223, both driven by a FGFR2 amplification; AN3CA (endometrial carcinoma) bearing a mutated FGFR2; the acute myeloid leukemia cell lines MOLM-13 and MV-4-11-B with FLT3 mutations; and the NSCLC adenocarcinoma LC-2/ad harboring a CCDC6-RET fusion. Potent kinase inhibition does not, however, strictly translate into antiproliferative activity, as demonstrated in the TRKA-dependent cell lines CUTO-3 and KM-12. Importantly, nintedanib treatment of NCI-H1703 tumor xenografts triggered effective tumor shrinkage, indicating a direct effect on the tumor cells in addition to the antiangiogenic effect on the tumor stroma. These findings will be instructive in guiding future genome-based clinical trials of nintedanib.

Introduction

The inhibition of tumor angiogenesis is an established therapeutic option in the treatment of cancer patients. Several small-molecule inhibitors, as well as antibodies, have been approved in recent years, starting with bevacizumab in 2004 - (Culy, 2005) for colorectal cancer and the latest additions of ramucirumab and nintedanib in 2014 (Reinmuth et al., 2015). Antiangiogenic treatments, except to treat renal cell carcinoma, are being combined with chemotherapy (Jayson et al., 2016; Stukalin et al., 2016) to enhance patient response and to prolong overall survival. The mechanism responsible for the enhanced efficacy of chemotherapeutic drugs is still not completely understood, especially since several components of the tumor stroma are involved that are not necessarily linked (Gasparini et al., 2005a,b; Boere et al., 2010; Moschetta et al., 2010; Jain, 2014). Hypotheses include tumor vessel normalization through antivascular effects, leading to better drug delivery and distribution (Jain, 2005; Cesca et al., 2016), and vessel co-option, the ability of tumors to hijack the existing vasculature in organs such as the lungs or liver (Kerbel, 2015). Another possible contribution comes through the inhibition of specific "off-target" kinases of antiangiogenic tyrosine kinase inhibitors (TKIs) that are often associated with the so-called multi-TKIs (e.g., pazopanib targeting Ret kinase). Nintedanib has been previously described as a triple angiokinase inhibitor targeting the tumor stroma and specifically the vasculature (Hilberg et al., 2008). Based on the inhibition profile, nintedanib was profiled as an inhibitor of

A.T.L. and R.C.D. received funding through the University of Colorado Lung Cancer SPORE (NIH/NCI P50 CA058187).
https://doi.org/10.1124/jpet.117.244129.
[S] This article has supplemental material available at jpet.aspetjournals.org.

ABBREVIATIONS: Akt, protein kinase B; AML, myeloid leukemia; ampl., amplification; DDR 1 and 2, discoidin domain receptor family member 1 and 2; DMSO, dimethylsulfoxide; ERK, extracellular regulated kinase; FGFR, fibroblast growth factor receptor; KD, knockdown; MAPK, mitogen-activated protein kinase; NSCLC, non–small cell lung cancer; PDGFR, platelet-derived growth factor receptor; RTK, receptor tyrosine kinase; TKI, tyrosine kinase inhibitor; TRKA, tropomyosin receptor kinase A; VEGFR, vascular endothelial growth factor receptor.

tumor angiogenesis in clinical trials that led to its regulatory approval as second-line adenocarcinoma non–small cell lung cancer (NSCLC) treatment in combination with docetaxel (Reck et al., 2014). Nintedanib shows the strongest benefit in patients with rapidly progressing tumors that either do not respond to first-line platinum-based chemotherapy or show progress within 6 months after initiation of first-line chemotherapy, which hints to a predominant antiangiogenic effect of nintedanib because such rapidly growing tumors depend heavily on oxygen supply and aerobic metabolism and therefore proper vascular connections (Hilberg et al., 2014) J Clin Oncol 32, 2014 (suppl; abst e22080) ASCO poster). The question of whether the extended nintedanib kinase inhibition profile can contribute to the observed clinical benefit by directly affecting tumor cell proliferation and survival remains pertinent. FGFR genetic alterations, such as mutations or amplifications or fusions, have been reported for the following cancers: bladder (FGFR3) (Cancer Genome Atlas Research, 2014b), endometrial (FGFR2) (Winterhoff and Konecny, 2017) and lung (FGFR1) (Weiss et al., 2010; Dienstmann et al., 2014), breast (FGFR1 and 2), gastric (FGFR2) (Cancer Genome Atlas Research, 2014a), lung and and glioma (FGFR3-TACC3 fusion) (Capelletti et al., 2014; Di Stefano et al., 2015). Genetic alterations of the PDGFRA gene occur in about 5% of gastrointestinal stromal tumors, and amplifications are present in 5%–10% of glioblastoma multiforme cases, in oligodendrogliomas, in esophageal squamous cell carcinoma, in artery intimal sarcomas, and in 2%–3% of NSCLC adenocarcinomas (Heldin, 2013).

Here we present data that clearly underline the potential of nintedanib, as a single agent, to directly inhibit tumor cell proliferation and survival. This effect of nintedanib can be seen over a wide range of tumor types and various genetic alterations ranging from mutations to amplifications, and it is also demonstrated in combinations with a small-molecule inhibitor targeting a tumor epigenetically. We also demonstrate that inhibition of a receptor tyrosine kinase (RTK) at the kinase level does not necessarily translate into a cellular effect. Collectively, our results provide a strong rationale for clinical investigations of nintedanib in specific subsets of oncogene-driven cancers.

Materials and Methods

Molecular Characterization of Cancer Cell Line Panel (Ricerca 240-OncoPanel)

Information on the Ricerca 240-OncoPanel can be found at: https://www.eurofinspanlabs.com/Catalog/Products/ProductDetails.aspx?prodId=YWEUPExy%2Fhg%3D and is represented in Supplemental Table 3. Relative copy number values were determined using the Affymetrix Genome-Wide Human SNP Array 6.0 platform. The analysis was performed using the CRMA v2 method (Bengtsson et al., 2009), followed by CBS segmentation, both implemented as part of the Aroma Project (http://www.aroma-project.org) (Bengtsson et al., 2008). Absolute copy numbers were calculated using the PICNIC algorithm (http://www.sanger.ac.uk/science/tools/picnic) (Greenman et al., 2010).

Mutation Analysis

Mutations were called after best practices as described, for instance, in Alioto et al. (2015). For RNA-seq data processing and gene expression quantification, libraries from polyA-enriched RNA (protocols Qiagen, Illumina) were sequenced on an Illumina HiSeq1500 using the paired-end protocol with 50 cycles and 25 million reads in average. Gene and transcript quantification was performed using SAMtools version 1.0 (Li et al., 2009) and Cufflinks version 2.0.2 (Trapnell et al., 2010). The molecular status of nintedanib target kinases in the Ricerca panel was determined as follows: Kinases with a relative copy number >4 were considered amplified. The threshold for overexpression for each kinase was defined by the respective mean over all cell lines within a tumor type plus twice the respective standard deviation. The functional impact of mutations was derived from the MutationAssessor (http://mutationassessor.org/) (Reva et al., 2011). Statistics calculations (Fisher test) were performed using the R open source programming language (www.r-project.org; R Core Team, 2016, R: A language and environment for statistical computing. R Foundation for Statistical Computing, Vienna, Austria. URL http://www.R-project.org/).

Molecular Characteristics of Human Tumor Samples

Gene expression and alteration frequencies (copy number, mutation) within the TCGA data set were analyzed using the cBio Portal online tools (www.cbioportal.org) (Cerami et al., 2012).

Kinase Assay

Kinase assays were performed at Thermo Fisher Life Technologies (Bothell, WA) using standard protocols (SelectScreen Biochemical Profiling Service, Thermo Fisher Scientific). ATP concentrations used were at the apparent K_m.

Z'-LYTE Assay Conditions. The compounds were screened in 1% dimethylsulffoxide (DMSO) (final concentration) in the well. For 10-point titrations, 3-fold serial dilutions were conducted from the starting concentration. All peptide/kinase mixtures were diluted to a 2× working concentration in the appropriate kinase buffer (see *Kinase-Specific Assay Conditions* section for a complete description in Supplemental Material). All ATP solutions were diluted to a 4× working concentration in kinase buffer (50 mM HEPES pH 7.5, 0.01% BRIJ-35, 10 mM $MgCl_2$, 1 mM EGTA). Apparent ATP K_m is previously determined using a Z'-LYTE assay. The development reagent is diluted in development buffer (see section *Kinase-Specific Assay Conditions: Direct and Cascade* for a complete description in Supplemental Material). Ten times novel PKC lipid mix: 2 mg/ml phosphatidyl serine, 0.2 mg/ml DAG in 20 mM HEPES, pH 7.4, 0.3% CHAPS.

Adapta Assay Conditions. The compounds were screened in 1% DMSO (final concentration) in the well. For 10-point titrations, 3-fold serial dilutions are conducted from the starting concentration. All substrate/kinase mixtures were diluted to a 2× working concentration in the appropriate kinase buffer (see *Kinase-Specific Assay Conditions* section for a complete description in Supplemental Material). All ATP solutions were diluted to a 4× working concentration in water. Apparent ATP K_m was previously determined using a radiometric assay except when no substrate was available, in which case an Adapta assay was conducted. The detection mix was prepared in TR-FRET dilution buffer. The detection mix consisted of EDTA (30 mM), Eu-anti-ADP antibody (6 nM), and ADP tracer. The detection mix contained the EC60 concentration of tracer for 5–150 μM ATP.

LanthaScreen Eu Kinase Binding Assay Conditions. The compounds were screened in 1% DMSO (final concentration) in the well. For 10-point titrations, 3-fold serial dilutions were conducted from the starting concentration. All kinase/antibody mixtures were diluted to a 2× working concentration in the appropriate kinase buffer (see *Kinase-Specific Assay Conditions* section for a complete description in Supplemental Material). The 4× AlexaFluor-labeled tracer was prepared in kinase buffer.

Cells and Western blotting

NCI-H1703 cells were seeded in six-well plates and reverse-transfected with 10 nmol/l of ON-TARGETplus Human siRNA and LipofectAMINE RNAiMAX (cat. no. 13778075; Invitrogen, Carlsbad, CA) for 72 hours at 37°C. Transfections were performed according to

the supplier's manual using the following siRNAs: (FGFR1 siRNA J-003131-00-0002-10; PDGFRA siRNA J-003162-00-0002-12; and nontargeting siRNA, D-001810-01-20), all obtained from Dharmacon (Cambridge, UK). Two hours before lysing the cells, nintedanib (BIBF 1120) and/or PD173074 was added in various concentrations to the cultures. Compounds in DMSO were diluted serially and incubated with the cells. Lysates were generated according to standard protocols (Ausubel et al., 2004) (Current Protocols in Molecular Biology, edited by F. M. Ausubel, R. Brent, R. E. Kingston, D. D. Moore, J. G. Seidman, J. A. Smith & K. Struhl, 2004, John Wiley and Sons, Inc.). Western blotting was done using standard SDS-PAGE methods, loading 10 μg of protein per lane, with detection by enhanced chemiluminescence. The amounts of total and phosphorylated proteins were detected using the corresponding antibodies, purchased and used according to the manufacturer's instructions: phospho-p44/42 mitogen-activated protein kinase (MAPK) (Erk1/2) (Thr202/Tyr204) (cat. no. 9101; Cell Signaling Technology, Danvers, MA); p44/42 MAPK (Erk1/2) (cat. no. 9102; Cell Signaling); protein kinase B (Akt) (cat. no. 9272); phosphorylated Akt (Ser473) (cat. no. 4058); cleaved caspase-3 (cat. no.. 9665); FGF receptor 1 (D8E4) XP Rabbit mAb (cat. no. 9740); FGF receptor 2 (D4H9) (cat. no. 11835); and PDGF receptor α (cat. no. 3164) were all obtained from Cell Signaling. GAPDH was used as a loading control (ab8245; Abcam, Cambridge, MA).

Cell Viability Assay

Between 3000 and 10,000 cells/well were plated in 96-well flat-bottom microtiter plates and incubated overnight at 37°C in a CO_2 incubator with the respective medium. Test compound was added at various concentrations for 72 hours. After 6-hour incubation with Alamar Blue solution (Thermo Fisher/Invitrogen, Carlsbad, CA) at 37°C, fluorescence was measured (Envision MultiModeReader; PerkinElmer, Waltham, MA) using an excitation wavelength of 531 nm and emission at 595 nm.

Data Analysis

Data were fitted by an iterative calculation using a sigmoidal curve analysis program (Prism version 3.0; Graph Pad, La Jolla, CA) with variable Hill slope from which EC_{50} values were calculated.

IncuCyte Assay

Acute myeloid leukemia (AML) cells (MOLM-13, MV-4-11B, and THP-1) were plated (1×10^4/well) in 96-well poly-D-lysine–coated black/clear bottom plates (BD BioCoat, Horsham, PA). The next day, compounds were added at the indicated concentrations. Visualization and measurement of cell growth were by IncuCyte ZOOM live cell imaging (Essen BioScience, Ann Arbor, MI). Cell confluence was monitored for up to 140 hours, during which time images were taken every 3 hours.

In Vivo Tumor Models

Mice were housed under pathogen-free conditions (American Association for Assessment of Laboratory Animal Care accredited facility) and treated according to the institutional, governmental, and European Union guidelines (Austrian Animal Protection Laws, Society of Laboratory Animal Science [GV-SOLAS], Federation of Laboratory Animal Science Associations [FELASA]). All animal studies were reviewed and approved by the internal ethics committee and the local governmental committee. Female mice 6 to 8 weeks old, BomTAC:NMRI-*Foxn1^{nu}* (21–31 g) were inoculated with 1×10^6 (in 100 μl) NCI-H1703 or 2.5×10^6 MV-4-11-B cells subcutaneously into the right flank. Tumors were measured three times weekly using calipers. Volumes were calculated according to the following formula: tumor volume = length $\times$ diameter $2 \times \pi/6$. Tumor growth inhibition (TGI) was calculated to the following formula:

$$TGI = 100 \times \{1 - [(treated_{final\ day} - treated_{day1})/(control_{final\ day} - control_{day1})]\}.$$

One-sided decreasing Mann-Whitney tests were used to compare tumor volumes (efficacy). The P values for the tumor volume assessment were adjusted for multiple comparisons according to Bonferroni-Holm. For all analyses, P values < 0.05 represented a statistically significant effect. Kaplan-Meier survival curves were calculated calculation using a curve analysis program (Prism version 3.0; Graph Pad).

Results

Nintedanib Shows Potent Inhibition of FGFR Tyrosine Kinases 1–3 and PDGFR Tyrosine Kinases α/β. A head-to-head comparison of nintedanib with in-class competitor molecules revealed that nintedanib is more potent and has a more balanced inhibition profile across the triple angiokinase panel. Nintedanib was compared with sunitinib, vandetanib, pazopanib, and cediranib based on the IC_{50} values determined in parallel assays (Table 1). For nintedanib, the previously reported potency on VEGFR1-3, PDGFRα and β, and FGFR1–3 could be replicated with IC_{50} values <100 nmol/l, with slightly lower IC_{50} values for VEGFR2 and 3 and PDGFRα and β (Hilberg et al., 2008). Sunitinib, vandetanib, pazopanib, and cediranib inhibit VEGFR-2 and -3 at concentrations <100 nmol/l, but their inhibition of PDGFR α and β is less potent, and there is a clear potency drop with respect to FGFR inhibition. The notable exception is cediranib, which exhibits inhibition across the FGFRs that is comparable to nintedanib. In this comparison, sorafenib is the least potent drug, with IC_{50} values ≥100 nmol/l across the tested kinase panel.

TABLE 1
Potent inhibition of triple angiokinase targets by nintedanib and competitor compounds

Kinase[a]	VEGFR			PDGFR		FGFR			
IC_{50} (nmol/l)	−1	−2	−3	α	β	−1	−2	−3	−4
Nintedanib	99	3	4	18	28	41	47	96	421
Sunitinib	629	96	63	71	38	531	184	559	2670
Sorafenib	765	100	274	174	1110	>10,000	994	>10,000	>10,000
Vandetanib	208	12	74	187	3190	804	149	970	9560
Pazopanib	171	19	94	173	62	321	353	904	1660
Cediranib	64	4	18	296	496	39	20	63	622

Performed at Invitrogen.
[a]Additional kinases tested: ABL1, ACVR1B (ALK4), AKT2 (PKBβ), AMPK A1/B1/G1, AURKA (Aurora A), CAMK1D (CaMKI delta), CDK2/cyclin A, CHEK1 (CHK1), CSNK1A1 (CK1 alpha 1), CSNK2A1 (CK2 alpha 1), EGFR (ErbB1), EPHB2, FGFR1, FRAP1 (mTOR), GSK3B (GSK3 beta), IGF1R, LCK, MAP2K1 (MEK1), MAP3K8 (COT), MAPK14 (p38 alpha), MAPKAPK2, MYLK2 (skMLCK), NEK2, PAK4, PDK1, PRKACA (PKA), RAF1 (cRAF) Y340D Y341D, ROCK2, SRPK2, STK3 (MST2), TBK1.

Nintedanib Potently Inhibits Oncogenic RTKs beyond FGFRs and PDGFRs. The previously reported kinase target spectrum presented nintedanib as a triple-angiokinase small-molecule TKI (Hilberg et al., 2008). To explore kinase inhibition beyond that described previously, nintedanib was tested on a much broader, 245-kinase panel. In addition to the 13 kinases that had been previously reported as nintedanib targets, we 21 additional kinases that are also inhibited by nintedanib, with IC_{50} values <100 nmol/l (Table 2). Among these newly identified targets are kinases well known to be deregulated through genetic alterations and thus may act as oncogenic drivers in human cancers. These include kinases altered in subsets of NSCLC, such as Ret (2 nmol/l; (Berge and Doebele, 2014) and tropomyosin receptor kinase A (TRKA) (35 nmol/l; (Marchetti et al., 2008). The kinases Abl1 and Kit (13 and 9 nmol/liter, respectively) are also known to be driving mutations in several tumor types, including leukemias (Greuber et al., 2013; Stankov et al., 2014). Nintedanib also inhibits DDR1 and 2 (23 and 18 nmol/l, respectively), which have been described as involved in inflammatory and fibrotic processes (Guerrot et al., 2011; Olaso et al., 2011).

The fact that TKIs interfere with kinase activity in in vitro kinase assays does not necessarily mean that this activity will translate into cellular activity. We addressed this issue in two cell lines with known rearrangements of *NTRK1* leading to constitutive TRKA receptor activation: the CUTO-3.29 NSCLC adenocarcinoma cell line bearing the MPRIP-NTRK1 rearrangement and (Doebele et al., 2015) and the microsatellite instability high colorectal cancer cell line KM-12, which has the TPM3-NTRK1 translocation (Camps et al., 2004). As shown in Fig. 1, the CUTO-3.29 (Fig. 1C) and KM12 (Fig. 1D) cells have high levels of Ptrka, resulting in elevated pERK1/2 and pAKT levels. As demonstrated, these pTRKA and pERK1/2 levels can be reduced by the addition of the TRK-specific inhibitor, entrectinib, at concentrations as low as 1 nmol/l. In contrast, much higher concentrations of nintedanib (≥1000 nmol/l) were required to reduce pTRKA and pERK1/2 levels. The EC_{50} values of nintedanib and entrectinib were calculated to be 955 and 117 nmol/l for the CUTO-3.29 cells and 557 and 2.3 nmol/l for the KM12 cell line, respectively (Fig. 1, A and B). Thus, although nintedanib is a relatively potent inhibitor of TRKA in the kinase panel, this potency does not translate into inhibition of receptor phosphorylation and downstream signaling in cancer cell lines bearing TRKA rearrangements.

TABLE 2

Extended in vitro kinase inhibition profile of nintedanib

Data were determined using the SelectScreen Biochemical Kinase Profiling Service and performed at Thermo Fisher Life Technologies. Measurements were performed in triplicate.

Kinase	IC_{50} (nmol/l)
ABL1	12 ± 5
BLK	42 ± 9
BTK	34 ± 14
CSF1R	5 ± 2
DDR1	17 ± 7
DDR2	16 ± 4
FYN	74 ± 24
JAK3	67 ± 27
KIT	6 ± 3
MAP3K3 (MEKK3)	58 ± 25
MAP3K7	46 ± 31
MELK	3 ± 2
MST4	84 ± 9
NTRK1 (TRKA)	30 ± 8
NTRK3 (TRKC)	48 ± 25
NUAK1	50 ± 8
RET	2 ± 1
SIK2	11 ± 4
STK24	61 ± 12
TGFBR1	77 ± 20
YES1	14 ± 4

Nintedanib Inhibits Tumor Cell Proliferation Directly. To address the cellular inhibitory capacity of nintedanib in more detail, the drug was tested on a large collection of cell lines (Ricerca 240-OncoPanel, Supplemental Table 3). Nintedanib displayed efficacy (cutoff: 500 nmol/l; Supplemental Table 1a) against 12 of the 242 cancer cell lines across several indications (Fig. 2A), including gastric carcinoma, chronic myelogenous leukemia, AML, NSCLC, renal cancer, rhabdomyosarcoma, and thyroid carcinoma (Supplemental Table 1b). These cell lines carry driver mutations that may, potentially, be targeted by nintedanib. For example, the AML cell line MV-4-11 expresses the mutated FLT3 ITD allele exclusively, which acts as the oncogenic driver (Quentmeier et al., 2003) and is inhibited by nintedanib with a GI_{50} of 53 nmol/l (Supplemental Table 1a). Of the 12 sensitive cell lines, 10 exhibited genetic alterations within a total number of 16 nintedanib target kinases, as mutation, amplification, or overexpression (Fig. 2B; Supplemental Table 2). The two sensitive cell lines that do not carry mutations in any of the nintedanib target kinases are the highly mutated A-427 (NSCLC) line that carries 418 mutations and the renal cell carcinoma cell line G-401 with 311 mutations (Supplemental Table 1a). In addition, the A-427 cell line shows a highly complex amplification pattern. The 16 kinase genes as shown in Fig. 2B are altered to a similar extent in both sensitive and insensitive cell lines.

The TCGA data sets for those tumor types represented by the sensitive cell lines was queried to determine the total frequency of alterations in the 16 nintedanib targetable kinases. Around 42% of gastric cancer cases harbored molecular alterations in any of the described 16 genes. The alterations detected in the acute myeloid leukemia and chronic lymphatic leukemia study were mostly mutations compared with amplifications or rearrangements (Supplemental Fig. 1). The kinases overexpressed in the nintedanib-sensitive cell lines were, to a certain extent, also overexpressed in the respective TCGA data sets (Supplemental Fig. 2). In summary, 8 of the 12 nintedanib-sensitive cell lines from the 242 cancers panel contained genetic alterations in kinases targeted by nintedanib.

Effects on Growth of Tumor Cell Lines In Vitro where Nintedanib Targets May be Driver Mutations. We determined the responses of the the NSCLC cell line NCI-H1703 (PDGFRα and FGFR1 ampl.), the gastric cancer line KatoIII (FGFR2 ampl.), the endometrial cancer cell line AN3CA (FGFR2 mut.), and the breast cancer cell line MFM-223 (FGFR2 ampl.) to treatment with nintedanib. As shown in Table 3, growth of all four cell lines was inhibited by nintedanib treatment with EC_{50} values in the lower nanomolar range: NCI-H1703 10 nmol/l, KatoIII 176 nmol/l, AN3CA 152 nmol/l, and MFM-223 108 nmol/liter. As expected, sorafenib, which is a very weak inhibitor of PDGFR and FGFR kinase activity (see Table 1), was also a weak inhibitor of the NCI-H1703 and KatoIII cell lines (EC_{50} values of 258 and

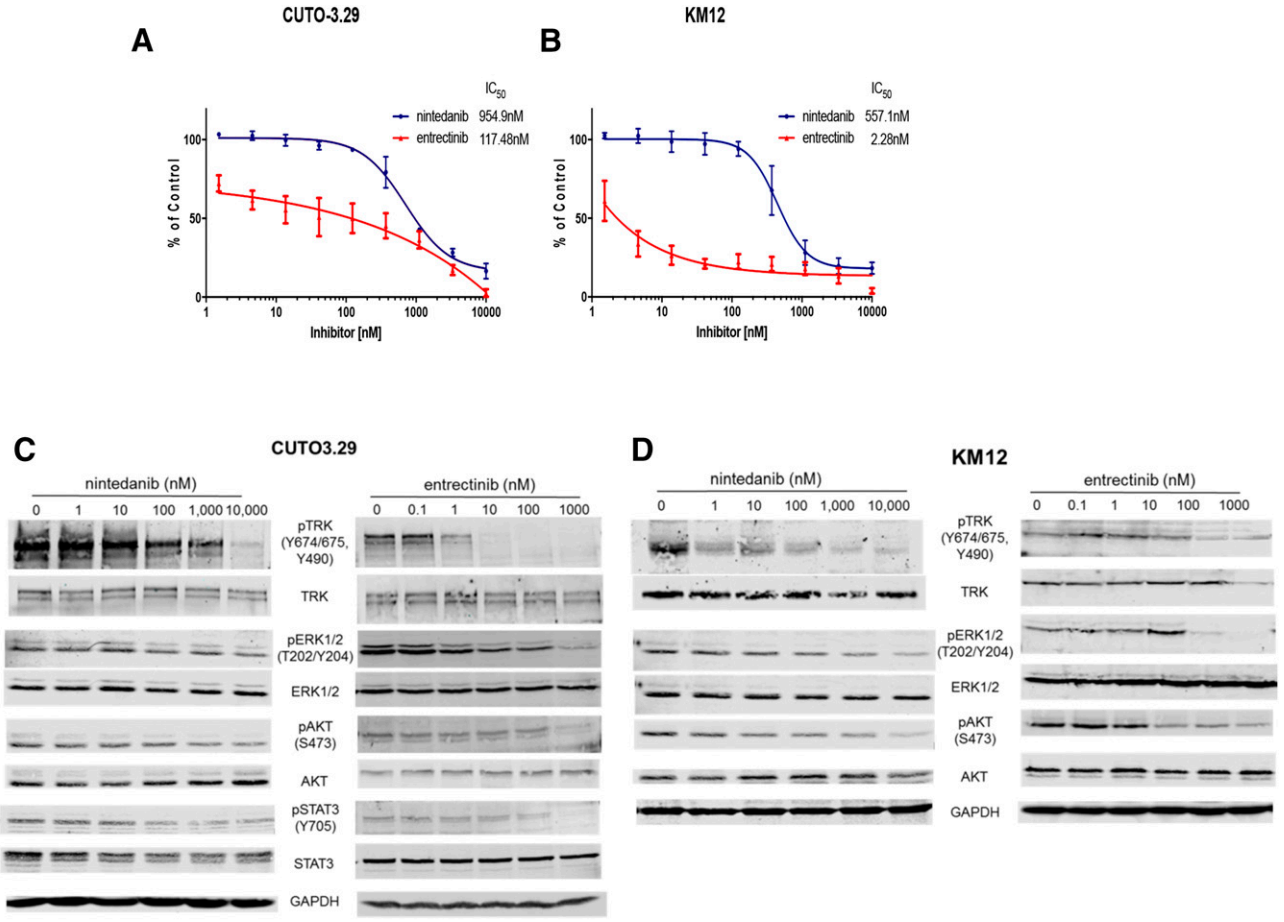

Fig. 1. Inhibition of proliferation and TRKA and downstream signaling of TRKA fusion cell lines using nintedanib and entrectinib. Human TRKA fusion cell lines CUTO3.29 (A) and KM12 (B) were treated with the indicated dose range of ninitedanib (blue) or entrectinib (red) and assayed for cell proliferation 72 hours after treatment using an MTS assay (n = 3, error bars represent ± S.E.M.). The IC_{50} was calculated for each cell line as follows: CUTO3.29 treated with nintedanib, 954.9 ± 7.2 nmol/l; or with entrectinib, 117.48 ± 5.6 nmol/liter; KM12 treated with nintedanib, 557.1 ± 5.6 nmol/l; and with entrectinib, 2.28 ± 0.3 nmol/l. CUTO3.29 (C) and KM12 (D) were treated with the indicated increasing doses of either nintedanib or entrectinib, and protein lysates were collected 2 hours later for Western blot analysis of phospho-TRKA and downstream signaling of phospho-ERK1/2, phospho-AKT and phospho-STAT3. Western blot images are representative of three independent experiments.

383 nmol/liter, respectively; Table 3). Sunitinib, which had IC_{50} values of 71 and 184 nmol/liter against PDGFRα and FGFR2 kinases respectively (Table 1), was also markedly less potent than nintedanib, with EC_{50} values of 39 nmol/l for the NCI-H1703 cells and 624 nmol/liter against the KatoIII line (Table 3). The differences between nintedanib, sunitinib, and sorafenib were confirmed by signaling pathway analysis in NCI-H1703 cells after PDGF BB stimulation. As shown in Fig. 3D, nintedanib and sunitinib were able to reduce pMAPK, pAKT, and pPDGFRα levels in a concentration-dependent manner down to 10–50 nmol/liter, whereas sorafenib was able to interfere fully with MAPK, AKT, and PDGFRα activation only at the highest tested concentration of 1 μmol/l.

Figure 3A also shows that activation of MAPK after stimulation with PDGF BB is inhibited by nintedanib at concentrations of ≥10 nmol/l. The same effect can be seen for phosphorylated AKT. In addition, the conversion of PARP to cleaved PARP as a marker of apoptosis is also seen at nintedanib concentrations ≥30 nmol/liter. In comparison, we also examined the effects of imatinib, a TKI that weakly inhibits PDGFR (Capdeville et al., 2002) in this setting. As shown in Fig. 3A, imatinib interferes with MAPK and AKT activation only at the highest concentration tested (1000 nmol/l), resulting in a faint cPARP signal. This difference between nintedanib and imatinib results from the lower (10-fold) potency of imatinib in inhibiting PDGFRB kinase activity, which is corroborated by the EC_{50} values of imatinib compared with those of nintedanib (shown in Table 3).

As shown in Supplemental Fig. 3, both the NCI-H1703 and KatoIII cell lines have two genetic amplifications. PDGFRA and FGFR1 are focally amplified in the NCI-H1703 cells, whereas FGFR2 and PDGFRA are amplified in the KatoIII cells. To determine which genetic alteration is driving the proliferation and survival in these two cell lines, knockdown experiments were performed. Figure 3B shows that knocking down FGFR1 in the NCI-H1703 cells had no effect on pAKT and pMAPK, whereas the PDGFRA knockdown (KD) reduced the pMAPK as well as the pAKT signal. The addition of increasing concentrations of nintedanib to the PDGFRA KD resulted in a complete loss of the pMAPK and pAKT signals. The addition of nintedanib to the FGFR1 KD also had an impact on the pAKT and MAPK signals but to a lesser extent, demonstrating that NCI-H1703 cells are driven primarily by PDGFRA amplification.

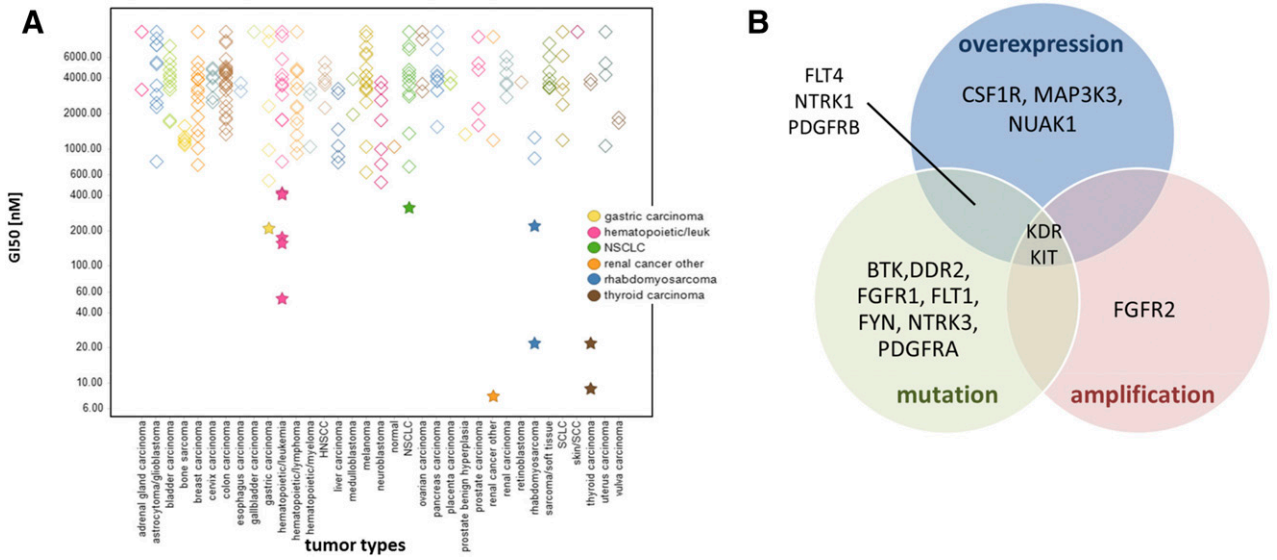

Fig. 2. Mutational analysis of nintedanib sensitive tumor cell lines. (A) Response of Ricerca 240-OncoPanel cell lines to nintedanib. *Sensitive cell lines ($GI_{50} \leq 500$ nmol/l). The color code legend highlights the tumor types represented by the sensitive cell lines. (B) Venn diagram showing the 16 genes and their respective alterations in the sensitive cell lines highlighted in (A).

Among the cancer indications with nintedanib-targetable driver mutations, gastric cancer shows an FGFR2 amplification prevalence of 4%–10% (Cancer Genome Atlas Research, 2014a). We analyzed the effects of nintedanib, as a representative of this group, on proliferation and survival pathways in the KatoIII cells. This cell line has been reported to have a copy number gain of 17 for FGFR2. Nintedanib inhibited proliferation in this cell line with an IC_{50} of 176 nmol/l and interfered with MAPK and AKT activation in bFGF- stimulated KatoIII cells down to 100 and 30 nmol/l, respectively (Fig. 3C). In the same experiment, the pan-FGFR inhibitor PD173074 inhibited KatoIII cell proliferation with an IC_{50} of 30 nmol/l and interfered with MAPK and AKT at a concentration as low as 10 nmol/l.

The NSCLC adenocarcinoma cell line LC-2/ad, which carries a CCDC6-RET fusion as a driver mutation (Suzuki et al., 2013), was also tested for its response to nintedanib, based on our finding that RET is also a target for the drug (EC_{50} value = 149 nmol/l). In the same experiment, vandetanib, a marketed drug for the treatment of thyroid carcinoma based on its Ret inhibition, gave an EC_{50} value of 247 nmol/l (data not shown).

Based on the previously reported inhibition of Flt3 by nintedanib (Kulimova et al., 2006; Hilberg et al., 2008) we were interested in exploring the combination with the small-molecule BET (bromodomain and extraterminal) family inhibitor BI 894999 (Effects of the novel BET inhibitor BI 894999 on upregulation of *HEXIM1* in cancer cells and on antitumor activity in xenograft tumor models. J Clin Oncol 34, 2016, suppl; abstract 11574 (ASCO)). As demonstrated in Supplemental Fig. 4, nintedanib specifically contributes to the inhibition of proliferation in Flt3-mutated AML cell lines (MOLM-13 and MV-4-11-B) but did not inhibit the proliferation of THP-1 AML cells carrying wild-type Flt3. The combination of nintedanib with BI 894999 completely inhibited the proliferation of MOLM-13 and MV-4-11-B AML cells, whereas no beneficial effect of the combination in the Flt3 wild-type cell line was seen (Fiskus et al., 2014).

In Vivo Antitumor Efficacy of Nintedanib in Tumor Xenografts Bearing Nintedanib-Targeted Driver Alterations. As nintedanib potently inhibited in vitro growth of the NCI-H1703 NSCLC cell line, which bears a PDGFRα amplification, we decided to analyze the in vivo antitumor efficacy in tumor-bearing mice. As demonstrated in Fig. 4, A and B, mice bearing subcutaneous NCI-H1703 tumors were treated with nintedanib (blocking VEGFR-2 and PDGFRs); vatalanib, a predominantly VEGFR-2 inhibiting TKI; and two different doses of the PDGFR inhibitor imatinib (75 mg/kg daily and twice daily). Selection of the doses of the drugs for the in vivo experiment was based on previously published reports demonstrating exposure of >1 μmol/l peak plasma concentrations with the selected doses of 100 mg/kg for

TABLE 3
Nintedanib potently inhibits the proliferation of cell lines carrying alterations in PDGFRA or FGFR2
Data were determined using an alamarBlue Cell Viability Assay Protocol from the Cell Proliferation Assay Protocols section of Life Technologies, drug exposure for 72 hours.

EC_{50} (nmol/l)	NCI-1703 PDGFRA ampl	KatoIII FGFR2 ampl.	AN3CA FGFR2 mut.	MFM-223 FGFR2 ampl.
Nintedanib	10 ± 3	176 ± 40	152 ± 22	108
PD173074	n.a.	30 ± 5	n.a.	n.a.
Imatinib	109 ± 65	n.a.	n.a.	n.a.
Sunitinib	39 ± 10	624 ± 85	n.a.	n.a.
Sorafenib	258 ± 25	383 ± 24	n.a.	n.a.

n.a., not applicable.

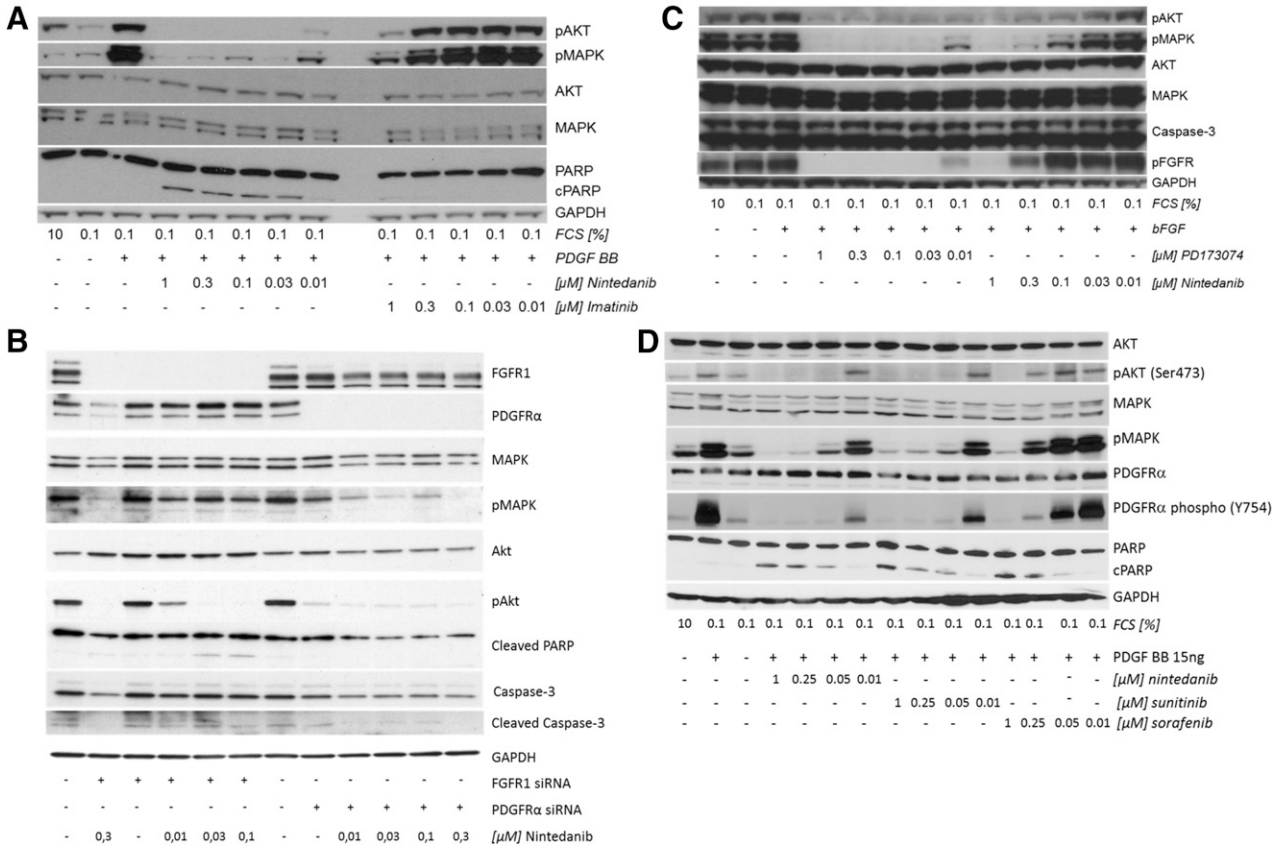

Fig. 3. Nintedanib inhibits ligand-dependent phosphorylation of MAPK and Akt in NCI-H1703 and KatoIII tumor cells. (A) NCI-H1703 Western blot analysis after exposure to either nintedanib or imatinib after stimulation with PDGF BB. Strong concentration-dependent reduction of phosphorylated MAPK and Akt levels by nintedanib compared with imatinib. (B) NCI-H1703 Western blot analysis after 72 hours of either FGFR1 or PDGFRA siRNA treatment and 2 hours of exposure to nintedanib shows concentration-dependent reduction of phosphorylated MAPK and Akt levels. Cleaved PARP and cleaved caspase-3 serve as indicators for apoptosis. Nintedanib concentrations are shown in micromoles per liter. (C) KatoIII Western blot analysis after exposure to either nintedanib or after stimulation with bFGF. Slightly stronger concentration-dependent reduction of phosphorylated MAPK and Akt levels by PD173074 compared with nintedanib. Western blot images are representative of three independent experiments. (D) NCI-H1703 Western blot analysis after exposure to nintedanib, sunitinib, or sorafenib after stimulation with PDGF BB. Concentration-dependent reduction of phosphorylated MAPK, Akt, and phosphor PDGFRα levels by nintedanib and sunitinib compared with sorafenib.

nintedanib (Hilberg et al., 2008) and vatalanib (Wood et al., 2000). In accordance with its in vitro activity on NCI-H1703 cells, nintedanib was the most potent of the three compounds in terms of its in vivo antitumor efficacy resulting in tumor shrinkage with a TGI value of 107% at 100 mg/kg. In comparison, the PDGFR inhibitor imatinib at 75 mg/kg either once or twice daily achieved TGI values of 45% and 58%, respectively. Once-daily treatment with vatalanib at a dose of 100 mg/kg resulted in a TGI of 73%, which is in line with the effects observed for antiangiogenic drugs. All treatments were well tolerated as demonstrated by the weight gain of all treatment groups over the treatment period (data not shown).

The anti-tumor efficacy of nintedanib alone and in combination with the BET family inhibitor BI 894999 was assessed in the subcutaneous MV-4-11-B AML model, as shown in Fig. 4, C–E. The TGI values for the single agent BET inhibitor BI 894999 were 78%, 92% for nintedanib, and 99% for the combination. The combination was well tolerated, and dosing could be maintained for almost 100 days as also shown in the Kaplan-Meyer plot in Fig. 4E. Seven of eight animals in the combination treatment group survived until the end of the experiment with only one treatment unrelated death. In the BI 894999 treatment group, all animals had to be euthanized according to termination criteria at around day 50, and in the nintedanib group, five animals were euthanized at day 100.

Discussion

The triple angiokinase inhibitor nintedanib has received regulatory approval for the treatment of idiopathic lung fibrosis, as well as for second line NSCLC in combination with docetaxel (Bronte et al., 2016). In this report, we present, for the first time, pharmacologic evidence that nintedanib directly and potently inhibits growth of tumors that are driven by genetic alterations in nintedanib target kinases. A screen of 240 tumor cell lines revealed 12 nintedanib- sensitive cell lines, nearly half of which were derived from leukemias. The 16 nintedanib-sensitive kinases were amplified, mutated, or overexpressed in these cell lines. None of the mutations represent known functional hotspots in the respective kinase domains, and their functional impact is, as yet, unknown; however, the activating nature of mutations outside the kinase domain has, for example, been demonstrated for PI3 kinase (Kang et al., 2005). The two cell lines that did not exhibit mutations in the nintedanib target genes showed multiple mutations and amplification patterns that were too

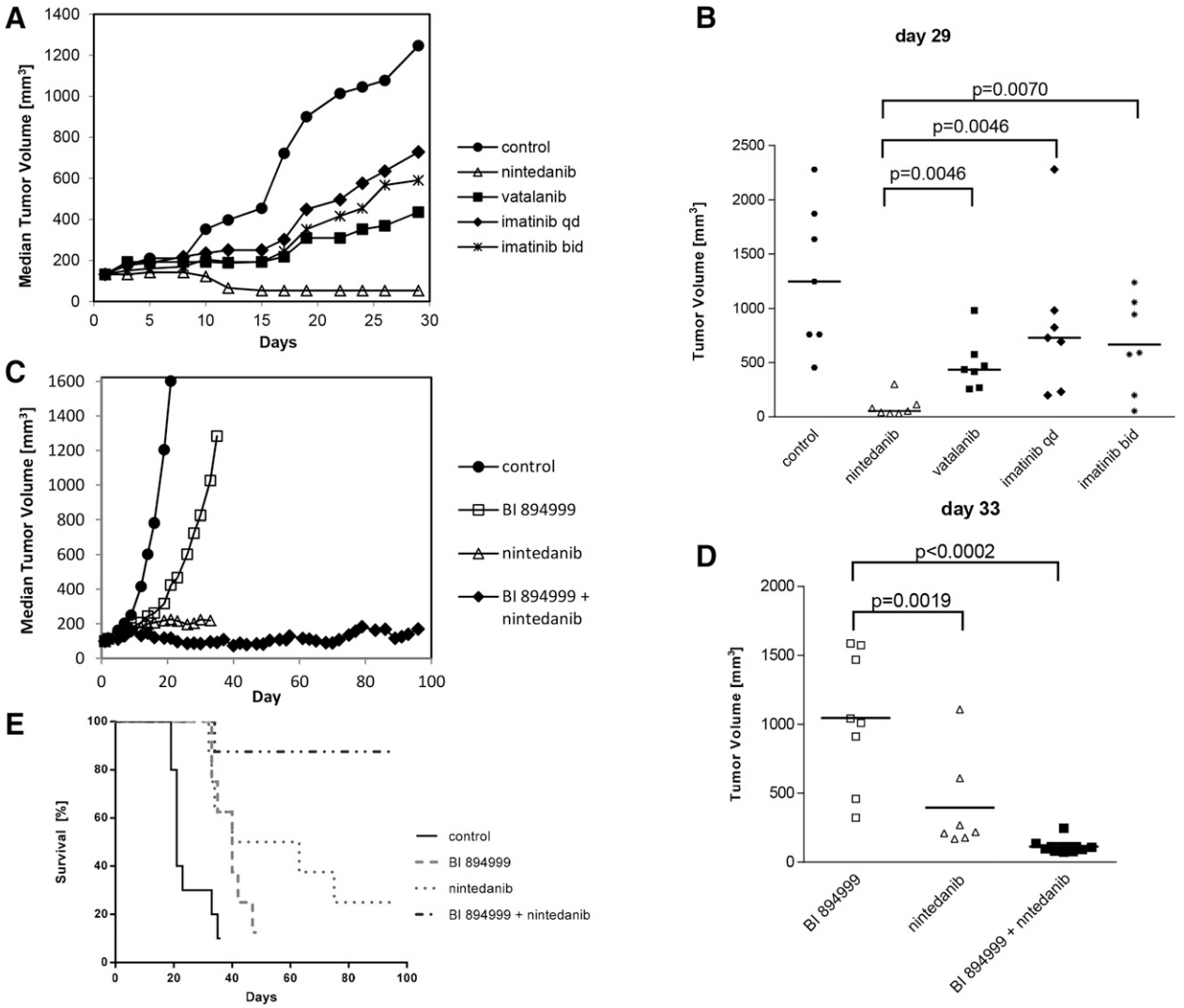

Fig. 4. Single-agent nintedanib induces tumor shrinkage of subcutaneous NCI-H1703 tumors. (A) Median tumor volume over time, (B) Single tumor volumes + median at day 29; nintedanib, 100 mg/kg daily (open triangles); vatalanib, 100 mg/kg daily (stars); imatinib, 75 mg/kg daily (filled triangles); and imatinib, 75 mg/kg twice daily (filled diamonds) (n = 7). Nintedanib in combination with the BET inhibitor BI894999 shows excellent antitumor efficacy, with seven of eight animals surviving ≥100 days. (C) Median tumor volume over time. (Nintedanib-treated animals euthanized prematurely because of tumor necrosis.) (D) Single tumor volumes + median at day 33. (E) Survival probability (n = 8 for treatment, n = 10 for vehicle control). Xenografts were established subcutaneously in athymic mice and allowed to reach a volume of ~100 mm^3 before treatment.

complex to derive clear sensitivity determinants for nintedanib. Alterations to the 16 nintedanib-sensitive kinases are not exclusive to the sensitive cell lines; they are also present in the insensitive cell lines, which we assume depend on other alterations and combinations to drive malignant behavior.

The TCGA database was interrogated for a combined aberration incidence for these kinases. The highest percentage (42.2%) was observed for gastric cancer, followed by AML (10%). FLT4 and PDGFRB are frequently overexpressed in gastric cancer and AML, indicating that nintedanib might be useful in the treatment of these particular patient populations.

This is potentially important in a scientific or clinical environment where tumor treatment is becoming increasingly fragmented based on the genetic information acquired through analysis of pretreatment tumor biopsies. This approach is now well established in the treatment of NSCLC patients bearing EML-ALK or EGFR mutations (Rocco et al., 2016), who receive appropriate TKIs targeting these alterations in the first line setting. Mutational screening of cancer is increasingly becoming incorporated into standard clinical practice requiring an increased need for targeted and well tolerated drugs. As demonstrated in this report, beyond potently inhibiting tumor angiogenesis, nintedanib also effectively blocks the proliferation of tumor cells driven by alterations in PDGFRA, FGFR2, RET, and FLT3. We show that this antiproliferative activity also translates into robust single-agent in vivo antitumor efficacy on treatment with nintedanib, including tumor shrinkage.

These results show that nintedanib has a dual mechanism: on the one hand, it suppresses tumor angiogenesis; on the other hand, it interferes directly with tumor cell proliferation, resulting in the induction of apoptosis. This opens new treatment possibilities for nintedanib in tumor subtypes, depending on PDGFRA, FGFR2, RET, or FLT3 genetic alterations either alone or in combination with chemotherapy.

AML associated with an internal tandem duplication of the *FLT3* gene (*FLT3* ITD mutation) has been reported to occur in about 20% of AML patients (Döhner et al., 2015). It is associated with unfavorable outcome, and patients are likely to relapse. A new class of compounds, BET inhibitors, are being intensively investigated preclinically and in phase 1 trials in AML. Combining the BET inhibitor BI 894999 with nintedanib may lead to improved survival benefit with good tolerability in the FLT3 mutant subgroup of AML. These findings extend a previous report on combining a BET inhibitor with a FLT3 tyrosine kinase inhibitor in an in vitro setting (Fiskus et al., 2014).

In clinical practice, nintedanib has demonstrated good tolerability and easy patient management. Here we show that nintedanib is a potent and well-balanced triple angiokinase inhibitor compared with other in-class competitors. Across the board of VEGFR, PDGFR, and FGFR isoforms constituting the triple angiokinase inhibition profile, nintedanib exhibits low nanomolar IC_{50} values, whereas competitors such as sunitinib, vandetanib, pazopanib, and sorafenib completely lack FGFR activity and are less potent inhibitors of VEGFR1-3 and PDGFR α and β. Despite extending the kinase inhibition profile to 34 kinases as targets for nintedanib, the drug is well tolerated by patients on a daily-dosing schedule as compared with in-class drugs that require intermittent dosing regimens to minimize adverse effects (Lee and Motzer, 2015). Furthermore, nintedanib has not been associated with serious side effects such as hand-foot syndrome (Li et al., 2015).

More FGFR selective TKIs (e.g., AZD4547, BGJ398) in cancer treatment have demonstrated promising clinical efficacies in phase 2 clinical trials but are also associated with notable adverse effects, such as hand-foot syndrome and serous retinopathy (Katoh, 2016). Hibi et al. have addressed the effects of nintedanib in FGFR1 amplified human lung squamous cell carcinoma cell lines H520 and LK-2 and could demonstrate that nintedanib inhibited the proliferation of FGFR1 CNG-positive LSCC cell lines in association with attenuation of the FGFR1-ERK signaling pathway in vitro and in vivo (Hibi et al., 2016). These data, together with the results presented in this article, demonstrate the potential of nintedanib as a potent inhibitor of cancer cells bearing FGFR alterations (amplifications, mutations) that warrants confirmation in clinical trials investigating nintedanib in cancer patients whose tumors harbor FGFR alterations.

Nintedanib's dual activity as a TKI targeting both genetic alterations in tumor cells (FGFRs and PDGFRs), as well as the tumor stroma by interfering with tumor angiogenesis, may represent an advantage over drugs that target specific RTKs more selectively. The importance of normalizing the tumor stromal environment becomes ever more important in the context of the upcoming combinations with immune-checkpoint inhibitors (Hendry et al., 2016). Emerging strong data underscore the importance of improving the immune response by interfering with the VEGF-driven negative effects on dendritic cell maturation, T-cell activation, regulatory T-cell proliferation, and promotion of myeloid-derived suppressor cells, as well as interfering with the activated tumor vessels and normalizing the tumor vessel bed (Hendry et al., 2016).

The fact that 34 kinases are inhibited at concentrations below 100 nmol/l identifies nintedanib as a multi TKI, but this fact is somewhat misleading because mere kinase inhibition does not always translate into inhibitory activity in a cellular context. In this article, we clearly showed that the kinase inhibition of NTRK1 with an IC_{50} value of 30 nmol/l did not translate into the cellular inhibition of cell lines harboring a TRKA receptor activation. The same discrepancy between kinase and cellular activity has already been observed for LYN and LCK kinases, with a much weaker cellular activity observed as would have been predicted from the kinase inhibition data (Hilberg et al., 2008).

Nintedanib has been demonstrated to be a potent anti-angiogenic and antifibrotic drug that has received regulatory approval as an anticancer agent and as an antifibrotic drug for the second-line treatment of NSCLC, in combination with docetaxel and idiopathic lung fibrosis, respectively. The additional features described in this report, namely the antiproliferative activity in tumors driven by PDGFR, FGFR, FLT3, and RET alterations, can be considered a future added value for nintedanib's clinical applications in cancer treatment. Similar approaches are already implemented in clinical practice for lung tumors driven by EML-ALK rearrangements (Blackhall and Cappuzzo, 2016) or RET-mutated thyroid carcinomas for crizotinib and vandetanib, respectively (Chu et al., 2012). Nintedanib is already being tested clinically in some of these subindications with data becoming available in the coming years (e.g., NCT02278978, NCT02299141).

Acknowledgments

The authors thank Monika Kriz, Matthew Kennedy, Martina Scherer, Regina Ruzicka, Nina Rodi, Susanne Schmittner, and Susy Straubinger for excellent technical assistance and data evaluation and to Dr. Elizabeth Anderson for critical reading of the manuscript.

Authorship Contribution

Participated in research design: Hilberg, Tontsch-Grunt, Baum, Le, Doebele, Lieb, Gianni, Voss, Garin-Chesa, Haslinger, Kraut.

Conducted experiments: Tontsch-Grunt, Baum, Le, Lieb, Gianni, Voss.

Performed data analysis: Hilberg, Tontsch-Grunt, Baum, Le, Doebele, Lieb, Gianni, Voss, Garin-Chesa, Haslinger.

Wrote or contributed to the writing of the manuscript: Hilberg, Tontsch-Grunt, Baum, Le, Doebele, Lieb, Gianni, Voss, Garin-Chesa, Haslinger, Kraut.

References

Alioto TS, Buchhalter I, Derdak S, Hutter B, Eldridge MD, Hovig E, Heisler LE, Beck TA, Simpson JT, Tonon L, et al. (2015) A comprehensive assessment of somatic mutation detection in cancer using whole-genome sequencing. *Nat Commun* **6**: 10001.

Bengtsson H, Irizarry R, Carvalho B, and Speed TP (2008) Estimation and assessment of raw copy numbers at the single locus level. *Bioinformatics* **24**:759–767.

Bengtsson H, Wirapati P, and Speed TP (2009) A single-array preprocessing method for estimating full-resolution raw copy numbers from all Affymetrix genotyping arrays including GenomeWideSNP 5 & 6. *Bioinformatics* **25**:2149–2156.

Berge EM and Doebele RC (2014) Targeted therapies in non-small cell lung cancer: emerging oncogene targets following the success of epidermal growth factor receptor. *Semin Oncol* **41**:110–125.

Blackhall F and Cappuzzo F (2016) Crizotinib: from discovery to accelerated development to front-line treatment. *Ann Oncol* **27** (Suppl 3):iii35–iii41.

Boere IA, Hamberg P, and Sleijfer S (2010) It takes two to tango: combinations of conventional cytotoxics with compounds targeting the vascular endothelial growth factor-vascular endothelial growth factor receptor pathway in patients with solid malignancies. *Cancer Sci* **101**:7–15.

Bronte G, Passiglia F, Galvano A, Barraco N, Listì A, Castiglia M, Rizzo S, Fiorentino E, Bazan V, and Russo A (2016) Nintedanib in NSCLC: evidence to date and place in therapy. *Ther Adv Med Oncol* **8**:188–197.

Camps J, Morales C, Prat E, Ribas M, Capellà G, Egozcue J, Peinado MA, and Miró R (2004) Genetic evolution in colon cancer KM12 cells and metastatic derivates. *Int J Cancer* **110**:869–874.

Cancer Genome Atlas Research Network (2014a) Comprehensive molecular characterization of gastric adenocarcinoma. *Nature* **513**:202–209.

Cancer Genome Atlas Research Network (2014b) Comprehensive molecular characterization of urothelial bladder carcinoma. *Nature* **507**:315–322.

Capdeville R, Buchdunger E, Zimmermann J, and Matter A (2002) Glivec (STI571, imatinib), a rationally developed, targeted anticancer drug. *Nat Rev Drug Discov* **1**: 493–502.

Capelletti M, Dodge ME, Ercan D, Hammerman PS, Park SI, Kim J, Sasaki H, Jablons DM, Lipson D, Young L, et al. (2014) Identification of recurrent FGFR3-TACC3 fusion oncogenes from lung adenocarcinoma. *Clin Cancer Res* **20**: 6551–6558.

Cerami E, Gao J, Dogrusoz U, Gross BE, Sumer SO, Aksoy BA, Jacobsen A, Byrne CJ, Heuer ML, Larsson E, et al. (2012) The cBio cancer genomics portal: an open platform for exploring multidimensional cancer genomics data. *Cancer Discov* **2**: 401–404.

Cesca M, Morosi L, Berndt A, Fuso Nerini I, Frapolli R, Richter P, Decio A, Dirsch O, Micotti E, Giordano S, et al. (2016) Bevacizumab-induced inhibition of angiogenesis promotes a more homogeneous intratumoral distribution of paclitaxel, improving the antitumor response. *Mol Cancer Ther* **15**:125–135.

Chu CT, Sada YH, and Kim ES (2012) Vandetanib for the treatment of lung cancer. *Expert Opin Investig Drugs* **21**:1211–1221.

Culy C (2005) Bevacizumab: antiangiogenic cancer therapy. *Drugs Today (Barc)* **41**: 23–36.

Dienstmann R, Rodon J, Prat A, Perez-Garcia J, Adamo B, Felip E, Cortes J, Iafrate AJ, Nuciforo P, and Tabernero J (2014) Genomic aberrations in the FGFR pathway: opportunities for targeted therapies in solid tumors. *Ann Oncol* **25**:552–563.

Di Stefano AL, Fucci A, Frattini V, Labussiere M, Mokhtari K, Zoppoli P, Marie Y, Bruno A, Boisselier B, Giry M, et al. (2015) Detection, characterization, and inhibition of FGFR-TACC fusions in IDH wild-type glioma. *Clin Cancer Res* **21**: 3307–3317.

Doebele RC, Davis LE, Vaishnavi A, Le AT, Estrada-Bernal A, Keysar S, Jimeno A, Varella-Garcia M, Aisner DL, Li Y, et al. (2015) An oncogenic NTRK fusion in a patient with soft-tissue sarcoma with response to the tropomyosin-related kinase inhibitor LOXO-101. *Cancer Discov* **5**:1049–1057.

Döhner H, Weisdorf DJ, and Bloomfield CD (2015) Acute myeloid leukemia. *N Engl J Med* **373**:1136–1152.

Fiskus W, Sharma S, Qi J, Shah B, Devaraj SG, Leveque C, Portier BP, Iyer S, Bradner JE, and Bhalla KN (2014) BET protein antagonist JQ1 is synergistically lethal with FLT3 tyrosine kinase inhibitor (TKI) and overcomes resistance to FLT3-TKI in AML cells expressing FLT-ITD. *Mol Cancer Ther* **13**:2315–2327.

Gasparini G, Longo R, Fanelli M, and Teicher BA (2005a) Combination of antiangiogenic therapy with other anticancer therapies: results, challenges, and open questions. *J Clin Oncol* **23**:1295–1311.

Gasparini G, Longo R, Toi M, and Ferrara N (2005b) Angiogenic inhibitors: a new therapeutic strategy in oncology. *Nat Clin Pract Oncol* **2**:562–577.

Greenman CD, Bignell G, Butler A, Edkins S, Hinton J, Beare D, Swamy S, Santarius T, Chen L, Widaa S, et al. (2010) PICNIC: an algorithm to predict absolute allelic copy number variation with microarray cancer data. *Biostatistics* **11**: 164–175.

Greuber EK, Smith-Pearson P, Wang J, and Pendergast AM (2013) Role of ABL family kinases in cancer: from leukaemia to solid tumours. *Nat Rev Cancer* **13**: 559–571.

Guerrot D, Kerroch M, Placier S, Vandermeersch S, Trivin C, Mael-Ainin M, Chatziantoniou C, and Dussaule JC (2011) Discoidin domain receptor 1 is a major mediator of inflammation and fibrosis in obstructive nephropathy. *Am J Pathol* **179**:83–91.

Heldin CH (2013) Targeting the PDGF signaling pathway in tumor treatment. *Cell Commun Signal* **11**:97.

Hendry SA, Farnsworth RH, Solomon B, Achen MG, Stacker SA, and Fox SB (2016) The role of the tumor vasculature in the host immune response: implications for therapeutic strategies targeting the tumor microenvironment. *Front Immunol* **7**: 621.

Hibi M, Kaneda H, Tanizaki J, Sakai K, Togashi Y, Terashima M, De Velasco MA, Fujita Y, Banno E, Nakamura Y, et al. (2016) FGFR gene alterations in lung squamous cell carcinoma are potential targets for the multikinase inhibitor nintedanib. *Cancer Sci* **107**:1667–1676.

Hilberg F, Roth GJ, Krssak M, Kautschitsch S, Sommergruber W, Tontsch-Grunt U, Garin-Chesa P, Bader G, Zoephel A, Quant J, et al. (2008) BIBF 1120: triple angiokinase inhibitor with sustained receptor blockade and good antitumor efficacy. *Cancer Res* **68**:4774–4782.

Jain RK (2005) Antiangiogenic therapy for cancer: current and emerging concepts. *Oncology (Williston Park)* **19** (4, Suppl 3):7–16.

Jain RK (2014) Antiangiogenesis strategies revisited: from starving tumors to alleviating hypoxia. *Cancer Cell* **26**:605–622.

Jayson GC, Kerbel R, Ellis LM, and Harris AL (2016) Antiangiogenic therapy in oncology: current status and future directions. *Lancet* **388**:518–529.

Kang S, Bader AG, and Vogt PK (2005) Phosphatidylinositol 3-kinase mutations identified in human cancer are oncogenic. *Proc Natl Acad Sci USA* **102**:802–807.

Katoh M (2016) FGFR inhibitors: effects on cancer cells, tumor microenvironment and whole-body homeostasis (Review). *Int J Mol Med* **38**:3–15.

Kerbel RS (2015) A decade of experience in developing preclinical models of advanced- or early-stage spontaneous metastasis to study antiangiogenic drugs, metronomic chemotherapy, and the tumor microenvironment. *Cancer J* **21**: 274–283.

Kulimova E, Oelmann E, Bisping G, Kienast J, Mesters RM, Schwäble J, Hilberg F, Roth GJ, Munzert G, Stefanic M, et al. (2006) Growth inhibition and induction of apoptosis in acute myeloid leukemia cells by new indolinone derivatives targeting fibroblast growth factor, platelet-derived growth factor, and vascular endothelial growth factor receptors. *Mol Cancer Ther* **5**:3105–3112.

Lee CH and Motzer RJ (2015) Sunitinib as a paradigm for tyrosine kinase inhibitor development for renal cell carcinoma. *Urol Oncol* **33**:275–279.

Li H, Handsaker B, Wysoker A, Fennell T, Ruan J, Homer N, Marth G, Abecasis G, and Durbin R; 1000 Genome Project Data Processing Subgroup (2009) The sequence alignment/Map format and SAMtools. *Bioinformatics* **25**:2078–2079.

Li Y, Gao ZH, and Qu XJ (2015) The adverse effects of sorafenib in patients with advanced cancers. *Basic Clin Pharmacol Toxicol* **116**:216–221.

Marchetti A, Felicioni L, Pelosi G, Del Grammastro M, Fumagalli C, Sciarrotta M, Malatesta S, Chella A, Barassi F, Mucilli F, et al. (2008) Frequent mutations in the neurotrophic tyrosine receptor kinase gene family in large cell neuroendocrine carcinoma of the lung. *Hum Mutat* **29**:609–616.

Moschetta M, Cesca M, Pretto F, and Giavazzi R (2010) Angiogenesis inhibitors: implications for combination with conventional therapies. *Curr Pharm Des* **16**: 3921–3931.

Olaso E, Lin HC, Wang LH, and Friedman SL (2011) Impaired dermal wound healing in discoidin domain receptor 2-deficient mice associated with defective extracellular matrix remodeling. *Fibrogenesis Tissue Repair* **4**:5.

Quentmeier H, Reinhardt J, Zaborski M, and Drexler HG (2003) FLT3 mutations in acute myeloid leukemia cell lines. *Leukemia* **17**:120–124.

Reck M, Kaiser R, Mellemgaard A, Douillard JY, Orlov S, Krzakowski M, von Pawel J, Gottfried M, Bondarenko I, Liao M, et al.; LUME-Lung 1 Study Group (2014) Docetaxel plus nintedanib versus docetaxel plus placebo in patients with previously treated non-small-cell lung cancer (LUME-Lung 1): a phase 3, double-blind, randomised controlled trial. *Lancet Oncol* **15**:143–155.

Reinmuth N, Heigener D, and Reck M (2015) Novel angiogenesis inhibitors in non-small cell lung cancer. *Curr Opin Oncol* **27**:79–86.

Reva B, Antipin Y, and Sander C (2011) Predicting the functional impact of protein mutations: application to cancer genomics. *Nucleic Acids Res* **39**:e118.

Rocco G, Morabito A, Leone A, Muto P, Fiore F, and Budillon A (2016) Management of non-small cell lung cancer in the era of personalized medicine. *Int J Biochem Cell Biol* **78**:173–179.

Stankov K, Popovic S, and Mikov M (2014) C-KIT signaling in cancer treatment. *Curr Pharm Des* **20**:2849–2880.

Stukalin I, Alimohamed N, and Heng DY (2016) Contemporary treatment of metastatic renal cell carcinoma. *Oncol Rev* **10**:295.

Suzuki M, Makinoshima H, Matsumoto S, Suzuki A, Mimaki S, Matsushima K, Yoh K, Goto K, Suzuki Y, Ishii G, et al. (2013) Identification of a lung adenocarcinoma cell line with CCDC6-RET fusion gene and the effect of RET inhibitors in vitro and in vivo. *Cancer Sci* **104**:896–903.

Trapnell C, Williams BA, Pertea G, Mortazavi A, Kwan G, van Baren MJ, Salzberg SL, Wold BJ, and Pachter L (2010) Transcript assembly and quantification by RNA-Seq reveals unannotated transcripts and isoform switching during cell differentiation. *Nat Biotechnol* **28**:511–515.

Weiss J, Sos ML, Seidel D, Peifer M, Zander T, Heuckmann JM, Ullrich RT, Menon R, Maier S, Soltermann A, et al. (2010) Frequent and focal FGFR1 amplification associates with therapeutically tractable FGFR1 dependency in squamous cell lung cancer. *Sci Transl Med* **2**:62ra93.

Winterhoff B and Konecny GE (2017) Targeting fibroblast growth factor pathways in endometrial cancer. *Curr Probl Cancer* **41**:37–47.

Wood JM, Bold G, Buchdunger E, Cozens R, Ferrari S, Frei J, Hofmann F, Mestan J, Mett H, O'Reilly T, et al. (2000) PTK787/ZK 222584, a novel and potent inhibitor of vascular endothelial growth factor receptor tyrosine kinases, impairs vascular endothelial growth factor-induced responses and tumor growth after oral administration. *Cancer Res* **60**:2178–2189.

Address correspondence to: Frank Hilberg, Boehringer Ingelheim RCV GmbH Co KG, Dr. Boehringer-Gasse 5-11, A-1121 Vienna, Austria. E-mail: frank.hilberg@boehringer-ingelheim.com